Title

Direct Visualization of the Charge Transfer in a Graphene/α-RuCl3 Heterostructure via Angle-Resolved Photoemission Spectroscopy.

Journal

Nano Letters, 23(17)

Authors

Rossi, Antonio
Johnson, Cameron
Balgley, Jesse
et al.

Publication Date

2023-09-13

DOI

10.1021/acs.nanolett.3c01974

Peer reviewed

NANO LETTERS

pubs.acs.org/NanoLett
Letter

Direct Visualization of the Charge Transfer in a Graphene/α-$RuCl_3$ Heterostructure via Angle-Resolved Photoemission Spectroscopy

Antonio Rossi,* Cameron Johnson, Jesse Balgley, John C. Thomas, Luca Francaviglia, Riccardo Dettori, Andreas K. Schmid, Kenji Watanabe, Takashi Taniguchi, Matthew Cothrine, David G. Mandrus, Chris Jozwiak, Aaron Bostwick, Erik A. Henriksen,* Alexander Weber-Bargioni, and Eli Rotenberg

Cite This: *Nano Lett.* 2023, 23, 8000−8005

Read Online

ACCESS | Metrics & More | Article Recommendations | Supporting Information

ABSTRACT: We investigate the electronic properties of a graphene and α-ruthenium trichloride (α-$RuCl_3$) heterostructure using a combination of experimental techniques. α-$RuCl_3$ is a Mott insulator and a Kitaev material. Its combination with graphene has gained increasing attention due to its potential applicability in novel optoelectronic devices. By using a combination of spatially resolved photoemission spectroscopy and low-energy electron microscopy, we are able to provide a direct visualization of the massive charge transfer from graphene to α-$RuCl_3$, which can modify the electronic properties of both materials, leading to novel electronic phenomena at their interface. A measurement of the spatially resolved work function allows for a direct estimate of the interface dipole between graphene and α-$RuCl_3$. Their strong coupling could lead to new ways of manipulating electronic properties of a two-dimensional heterojunction. Understanding the electronic properties of this structure is pivotal for designing next generation low-power optoelectronics devices.

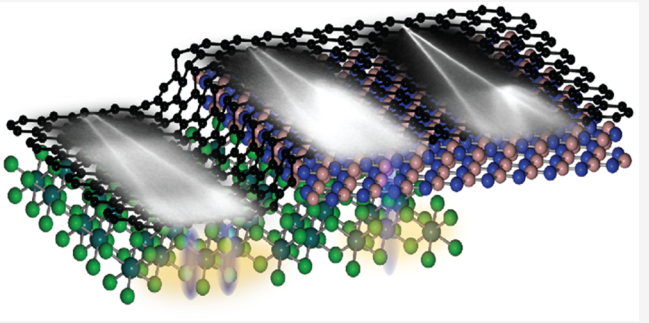

KEYWORDS: *Graphene, a-$RuCl_3$, p−n junction, electronic structure, angle-resolved photoemission spectroscopy, low energy electron microscopy*

In recent years, there has been a surge in interest in heterostructures composed of different two-dimensional (2D) materials.[1−3] These systems offer unique electronic properties that arise from their interfacial interactions, making them promising candidates for novel electronic and optoelectronic devices.[4,5] The absence of a covalent chemical bond between the layers opens the route toward designing 2D quantum systems that hold the promise to unlock the post-Moore era.[6,7] One particularly exciting development is the recent discovery of permanent charge transfer induced in graphene by proximity to α-$RuCl_3$ ($RuCl_3$ hereafter). In turn, this offers a route to explore the physics of charge-doped Mott insulators.[8−12]

$RuCl_3$ is a layered transition metal compound with a honeycomb lattice structure similar to graphene. However, unlike graphene, it is a Mott material with insulating behavior arising from strong electronic correlations.[13] At low temperatures, the complex competition of magnetic interactions ultimately stabilizes a zigzag antiferromagnet in $RuCl_3$.[14] However, the influence of doping, for instance by photo-induced charged carriers, is predicted to stabilize ferromagnetic order.[15] Additionally, $RuCl_3$ is classified as a Kitaev material due to its strong spin−orbit coupling, crystal field, and electronic correlations, which lead to anisotropic exchange interactions that favor the formation of a quantum spin liquid expected to host Majorana fermions.[16−20] These quasiparticles have non-Abelian statistics and are essential for topological quantum computation.[21] Nonetheless, the evidence for such behavior in $RuCl_3$ is still under debate[22] and seems to be strongly affected by the presence of crystal defects, which promote impurity scattering and non-Kitaev interactions.[23]

When graphene is brought in contact with $RuCl_3$, a charge transfer occurs between the two materials due to their different work functions and electronic structures.[8] This charge transfer can modify and hybridize the electronic properties of both materials[10] as well as influence the magnetism in $RuCl_3$.[15,24] The coupling between graphene and $RuCl_3$ can modify the electronic band structure of $RuCl_3$ and enhance its spin−orbit coupling, potentially impacting the Kitaev physics in the material.[9,24] Anomalous quantum oscillations have been

Received: May 26, 2023
Revised: August 21, 2023
Published: August 28, 2023

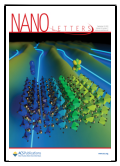

https://doi.org/10.1021/acs.nanolett.3c01974
Nano Lett. 2023, 23, 8000−8005

reported in the Gr/$RuCl_3$ heterostructure and explained within the Kitaev-Kondo lattice model.[25−27] The strong charge transfer has also been used to create modulation-doped graphene where a lateral thickness variation of a tunnel barrier changes the magnitude of the charge transfer between graphene and $RuCl_3$,[11] enabling ultrasharp (less than 5 nm wide) p−n junctions,[12] which were also observed in nanobubbles of graphene on $RuCl_3$.[28] The interaction between graphene and $RuCl_3$ can also lead to plasmon polaritons at the interface.[29] The coupling between plasmon polaritons and the Mott physics in $RuCl_3$ could unlock new ways of manipulating light and electronic properties, with potential applications in sensing, imaging, and communication. Moreover, by leveraging the unique passive doping control (no gating needed) of $RuCl_3$ over graphene, we envision the creation of low-power devices that exhibit enhanced light-harvesting capabilities and precise control over optical signals.[30]

Here, we employ a combination of experimental techniques to better investigate the electronic properties of the interface between $RuCl_3$ and graphene. Nanometer-scale spatially resolved photoemission spectroscopy (nanoXPS) and low-energy electron microscopy (LEEM) are used to explore the electronic properties of the heterostructure, allowing for a direct visualization of its charge transfer.

It is possible to effectively map the core levels of 2D systems and the dispersive electronic band structure of the heterostructure with submicron spatial resolution via nanoXPS and angle-resolved photoemission spectroscopy (nanoARPES).[31] LEEM allows imaging of the morphology and electronic properties of heterostructures with high spatial resolution. By using low-energy electrons to probe the surface of the material, we can investigate local variations in electronic properties to study their evolution over time. By comparing our experimental results with the calculations present in the literature, we validate our findings and provide a more complete understanding of the electronic properties of the heterostructure.

The experimental data show a massive charge transfer from graphene to $RuCl_3$, clearly visible in the nanoARPES data and reflected in the core levels measured via nanoXPS. LEEM analysis provides a value of the shift in work function that is much lower than the band shift measured via nanoARPES, consequent to the charge transfer between the layers. This discrepancy can be attributed to the presence of a dipole at the interface that greatly affects the work function value.[32] Moreover, the appearance of a band below the Fermi level, not observed in other ARPES experiments, can be attributed to the effect of charge transfer on $RuCl_3$. The most straightforward interpretation suggests that electrons from graphene have partially occupied the typically unoccupied upper Hubbard band, causing it to shift below the Fermi level. Alternatively, in a study of adatom-doped $RuCl_3$, Zhou et al. identified the appearance of such a band between the lower Hubbard band and Fermi level as an unconventional Mott transition driven by the charge transfer.[33] Either way, this new spectral weight shows that charge transfer from graphene to $RuCl_3$ induces significant changes in the electronic structure of the system. The presence of this band provides further evidence of the complex electronic interactions occurring at the interface and highlights the role of charge transfer in driving unconventional electronic phenomena in this system.

We fabricated a heterostructure composed of a thick hexagonal boron nitride (h-BN) substrate, with three other materials exfoliated on top: graphene, thin h-BN (2 nm), and $RuCl_3$ (Figure 1(a)). The fabrication and experimental details are reported in the Supporting Information. The device has three distinct regions: one with graphene on thick h-BN as a reference (Gr/h-BN), one with graphene directly on $RuCl_3$ (Gr/$RuCl_3$), and one with a thin h-BN flake sandwiched between graphene and $RuCl_3$ (Gr/h-BN/$RuCl_3$). The thin h-BN acts as a buffer to decrease the Gr-$RuCl_3$ interactions.[11,28] The thick h-BN substrate provides a stable and flat surface for other materials and minimizes the effect of the underlying substrate on the electronic properties of the heterostructure. A sketch of the three regions is reported in Figure 1(b) with a coherent color scheme. Figure 1(c) displays the heterostructure contour, where the contrast is given by the counts of the photoelectrons coming from the valence band of $RuCl_3$ at a binding energy of −1.3 eV. The contrast allows for identifying the three regions described above. The color scheme for the three colored squares on the map is consistent with the sketch in panel (b) and confirmed by the core level analysis via XPS. We focus on the peaks originating from Cl, Ru, and C core levels, reported in Figure 1(d,e). The most informative peak regarding the location of the $RuCl_3$ region is the Cl 2p core level. Its signal decreases when the h-BN buffer is present and

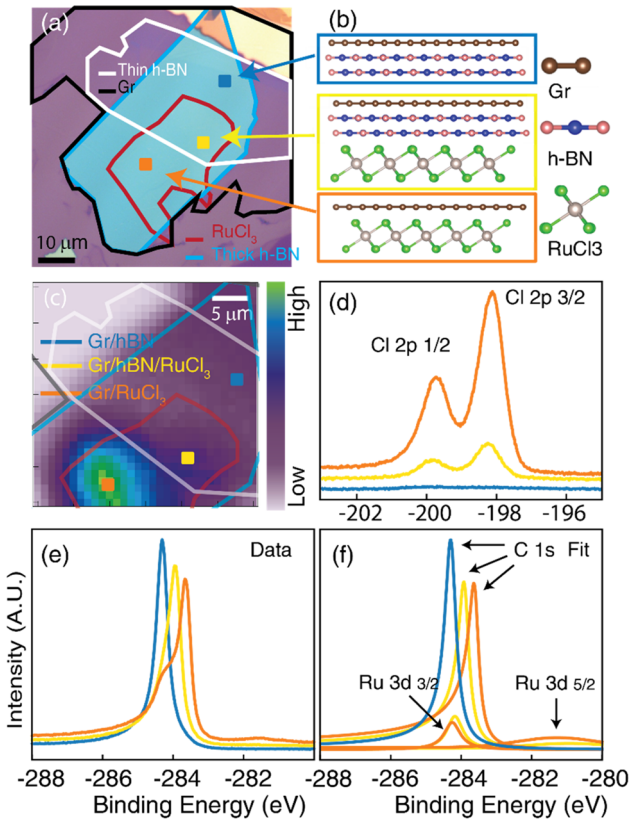

Figure 1. (a) Optical image of the analyzed device. False-color contours are used to highlight the different layers. (b) Sketch of the side view of three regions of interest. $RuCl_3$ must be considered as multiple layers, even though one layer is depicted for neatness. (c) Photoelectron intensity map collected at $E - E_F = -1.3$ eV. The colored profiles match the flakes highlighted in panel (a). (d) The Cl 2p core level collected in the regions highlighted in panel (c) with the corresponding color scheme. (e) Ru 3d and C 1s core levels collected from the same points of panel (d). (f) Fit of the Ru 3d and C 1s level for the data reported in panel (e).

https://doi.org/10.1021/acs.nanolett.3c01974
Nano Lett. 2023, 23, 8000−8005

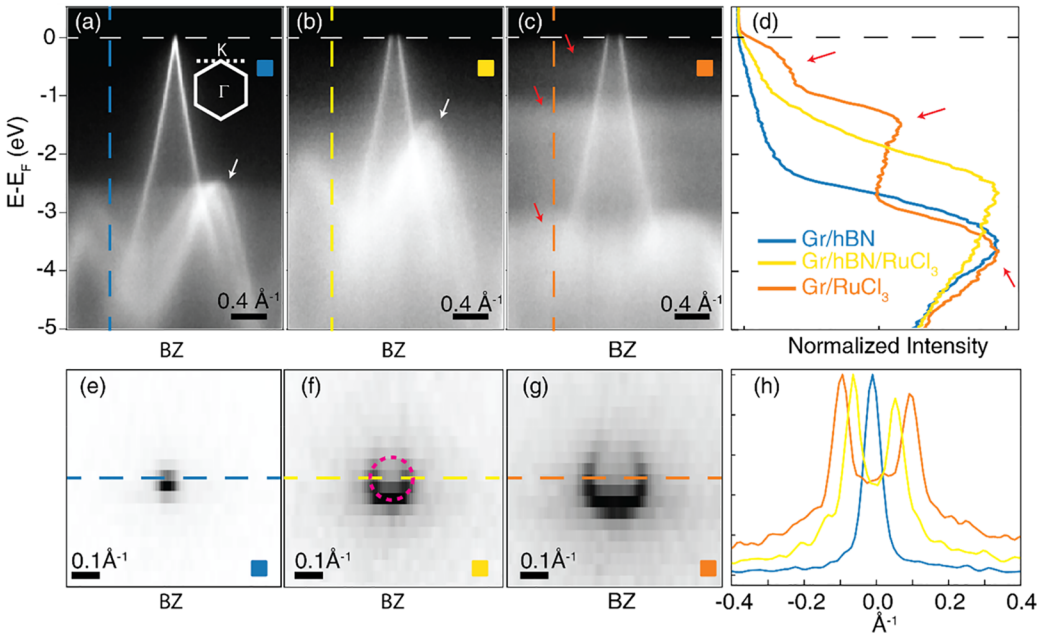

Figure 2. (a–c) Band structure collected around graphene K (point as depicted by panel (a) inset) from the three regions described above with a consistent color scheme. The horizontal dashed line is the Fermi level. The white arrows highlight the h-BN bands, the red arrows the $RuCl_3$ bands. (d) EDCs collected from panels (a–c) along the vertical dashed line. The red arrows highlight the corresponding states in panel (c). (e–g) Fermi surface of the band structure from the sample regions with the corresponding color scheme. The dashed red circle in panel (f) approximates the graphene Fermi surface. (h) MDCs collected across the dashed lines in panels (e–g).

disappears entirely outside the $RuCl_3$ flake. The Ru $3d_{3/2}$ core level partially overlaps with that of C 1s. It is possible to fit and track the evolution of the C 1s peak for the three different regions (Figure 1(f)). The fitting is performed considering one Doniach-Sunjic (DS) asymmetric line shape[34] for graphene and one DS for Ru $3d_{3/2}$, plus a Gaussian peak to take into account the broad and weak contribution from the $3d_{5/2}$ peak. While the Ru level remains roughly at fixed position, the C peak progressively shifts toward lower binding energy when increasing the coupling strength between graphene and $RuCl_3$. An overall shift of about −750 meV is observed for C 1s from the Gr/h-BN region. $RuCl_3$ is expected to induce a significant electron depletion in graphene[8,9] that is reflected on an electrostatic shift of the C core levels and the whole graphene band structure.

To directly visualize the electronic properties of the system, we conducted a nanoARPES study. This study enabled us to observe the electronic band structure in three specific regions highlighted in Figure 1(c). In Figure 2(a), we present the bands of the Gr/h-BN region, which are close to the neutrality point. In Figure 2(b,c), we show the band structures of the Gr/h-BN/$RuCl_3$ and Gr/$RuCl_3$ regions, respectively. Notably, the graphene bands in these regions are shifted upward by approximately 500 meV where the h-BN layers separate the graphene and $RuCl_3$ crystals and by 750 meV where $RuCl_3$ is in direct contact with graphene, indicating a progressive p-doping when reducing the distance between graphene and $RuCl_3$. The charge transfer from graphene to $RuCl_3$ is responsible for the shift of the Dirac cone and is similarly manifested in the position of the C 1s core level, where the observed chemical shift, as illustrated in Figure 1, can be also ascribed to the presence of an electrostatic dipole effect.[35] The influence of charge transfer and the resulting interface dipole is evident in the upward shift of the h-BN bands (indicated by white arrows) by approximately 1 eV, relative to the region without $RuCl_3$ as shown in Figure 2(a).

Because of the short mean free path of the photoelectrons, the $RuCl_3$ bands are visible only in the region where graphene is in direct contact, with no intervening h-BN buffer. The $RuCl_3$ bands are identified by studying the energy distribution curves (EDCs) taken along the dashed line in panels (a–c) of Figure 2 (Figure 2(d)). The $RuCl_3$ electronic structure, highlighted by three red arrows, displays two dispersionless bands centered at binding energies of ∼0.5 and ∼1.3 eV and a third more dispersive band at a deeper binding energy (∼3.8 eV).

The band centered at −1.3 eV is very likely to correspond to the lower Hubbard band, as indicated by Biswas et al.[9] However, it is worth noting that the observed energy position of the lower Hubbard band may appear to be lower than that predicted by computational models. This discrepancy could be attributed to the challenges in accurately estimating the energy gap using, e.g., density functional theory (DFT) calculations. Factors such as electron–electron interactions and correlation effects, which are not fully captured in DFT calculations, can influence the energy position of the lower Hubbard band.

Regarding the band at −3.8 eV, it is identified as an in-plane orbital and labeled as Cl p bands, originating from the Cl orbitals within the $RuCl_3$ structure.[33]

The presence of the band with spectral weight centered at about 0.5 eV below the Fermi level, which is typically not observed in ARPES experiments conducted on bulk $RuCl_3$,[33,36] suggests that its emergence is a result of the interaction between $RuCl_3$ and graphene. This band can be understood as the upper Hubbard band, which is typically unoccupied, being partially filled by electrons transferred from graphene and consequently shifted below the Fermi level. Another explanation put forth by Zhou et al. proposes that the introduction of dopants on the surface of $RuCl_3$ leads to the

https://doi.org/10.1021/acs.nanolett.3c01974
Nano Lett. 2023, 23, 8000–8005

population of new bands near the Fermi level.[33] These bands are attributed to an unconventional Mott transition, as described by the authors. It is possible that $RuCl_3$ undergoes a similar Mott transition when in contact with graphene, as observed in the case of Rb and K doping in ref 33.

A more quantitative estimate of the total amount of charge transferred between the layers, with and without the h-BN buffer layer, is given by considering the Fermi surface for each of the three regions, as reported in Figure 2(e−g). The Fermi surface of graphene exhibits a characteristic area of reduced intensity known as the "dark corridor". This phenomenon arises due to the interference of photoelectrons that are emitted from the two identical carbon atoms within each unit cell of graphene's honeycomb lattice.[37] The momentum distribution curves (MDCs) collected along the dashed lines on the Fermi surface are displayed in Figure 2(h). By fitting with two Lorentzian curves, the position of their maxima is used to evaluate the Fermi surface area, approximated as a circle. By means of the Luttinger theorem,[38−40] we can extract the amount of charge tunneling from graphene to $RuCl_3$, about 4.1×10^{13} cm^{-2}, consistent with previous, if indirect, experimental and computational observations.[8−10,24,29] When the spacing between layers is increased with a few h-BN layers, the tunnel barrier thickens, resulting in a decreased charge transfer and therefore a lower p-doping level in graphene (~1.7×10^{13} cm^{-2}).

Finally, we can quantify the electric dipole generated at the interface by the charge transfer to the $RuCl_3$. It is possible to compute the magnitude of the dipole by measuring the variation of the work function across the different regions of the system. By applying a positive voltage to the sample, the incident LEEM electrons transition from mirror mode, with the electrons reflecting before touching the sample surface, to LEEM mode, where the electrons are scattered from sample surface with a landing energy proportional to the applied sample bias. In LEEM mode, the incident electrons can be accepted into unoccupied bands of the sample surface causing a lower reflected intensity than in the mirror mode. The inflection point of this drop in intensity from mirror mode to LEEM mode can be interpreted as the work function of the sample surface when accounting for the work function of the LEEM cathode.

In Figure 3(a), selected LEEM images collected just below the mirror mode transition display the boundary of the three regions discussed above. The line profiles in Figure 3(b−d) show the average work function across each boundary in the directions indicated by the arrows in the corresponding LEEM images. The profile analysis highlights a difference in the work function of about 230 meV across the interface between Gr/$RuCl_3$ and Gr/h-BN. When the h-BN buffer layer is also present, the shift in the work function is reduced by 160 meV. This difference with respect to the Gr/h-BN region agrees with the 70 meV difference between the Gr/h-BN/$RuCl_3$ and Gr/$RuCl_3$ regions. Previously, Yu and co-workers demonstrated that the work function of graphene can be substantially affected by the dipole formed by surface adsorbates.[32] Analogously, here we estimate the magnitude of the electric field at the interface knowing the value of the chemical potential and the value of the work function, with respect to pristine graphene. In the presence of a dipole at the interface, the work function of graphene can be written as

$$W_{sample} = \Delta W_D + W^0_{gr} - E_F \quad (1)$$

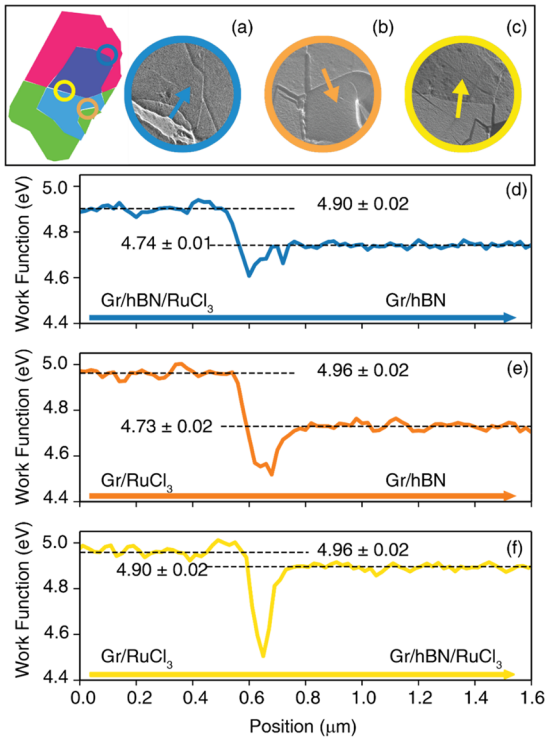

Figure 3. (a−c) Mirror mode LEEM images of selected regions of interest: (a) $RuCl_3$-hBN-Gr/Gr, (b) $RuCl_3$-Gr/Gr, (c) $RuCl_3$-Gr/$RuCl_3$-hBN-Gr. (d−f) Surface work function measured across the boundary separating the different regions along the arrows drawn in the microscopy panels.

where ΔW_D is the offset of work function due to the dipole at the interface, W^0_{gr} is the intrinsic work function of the undoped graphene, and E_F is the position of the Fermi level.[32] We can therefore evaluate the magnitude of the electric dipole with respect to the pristine sample simply considering the measured work function difference across the different regions and adding this to the corresponding difference in the E_F position with respect to the Dirac point. This results in an electric dipole energy of ~1 eV and ~660 meV for Gr/$RuCl_3$ and Gr/h-BN/$RuCl_3$ regions, respectively.

In conclusion, we used a combination of experimental techniques, including nanoXPS and nanoARPES and LEEM, to investigate the electronic properties of the Gr/$RuCl_3$ heterostructure. The results showed direct evidence of significant charge transfer from graphene to $RuCl_3$, leading to a doping-induced Mott transition and potential enhancement of the Kitaev physics. LEEM measurement also allowed us to provide an estimate of the dipole moment formed at the interface between $RuCl_3$ and graphene, instrumental for comprehensive device modeling. This work lays out valuable insights into the electronic properties of Gr/$RuCl_3$ heterostructures and its potential for future applications, where the passive control of the doping level in graphene is at the foundation of low-power electronics and light-harvesting devices.

■ ASSOCIATED CONTENT

Supporting Information

The Supporting Information is available free of charge at https://pubs.acs.org/doi/10.1021/acs.nanolett.3c01974.

https://doi.org/10.1021/acs.nanolett.3c01974
Nano Lett. 2023, 23, 8000−8005

Device fabrication methods including atomic force microscopy characterization of the device. Experimental details for nXPS and nARPES experiment including photon energy and light polarization used. LEEM measurements details (PDF)

AUTHOR INFORMATION

Corresponding Authors

Antonio Rossi − *Advanced Light Source and The Molecular Foundry, Lawrence Berkeley National Laboratory, Berkeley, California 94720, United States; Center for Nanotechnology Innovation @ NEST, Istituto Italiano di Tecnologia, Pisa 56127, Italy;* orcid.org/0000-0003-4574-7215; Email: antonio.rossi@iit.it

Erik A. Henriksen − *Department of Physics and Institute for Materials Science and Engineering, Washington University in St. Louis, St. Louis, Missouri 63130, United States;* orcid.org/0000-0002-4978-2440; Email: henriksen@wustl.edu

Authors

Cameron Johnson − *The Molecular Foundry, Lawrence Berkeley National Laboratory, Berkeley, California 94720, United States*

Jesse Balgley − *Department of Physics and Institute for Materials Science and Engineering, Washington University in St. Louis, St. Louis, Missouri 63130, United States*

John C. Thomas − *The Molecular Foundry, Lawrence Berkeley National Laboratory, Berkeley, California 94720, United States;* orcid.org/0000-0002-2151-7725

Luca Francaviglia − *The Molecular Foundry, Lawrence Berkeley National Laboratory, Berkeley, California 94720, United States*

Riccardo Dettori − *Physical and Life Sciences Directorate, Lawrence Livermore National Laboratory, Livermore, California 94550, United States;* orcid.org/0000-0002-4678-1098

Andreas K. Schmid − *The Molecular Foundry, Lawrence Berkeley National Laboratory, Berkeley, California 94720, United States*

Kenji Watanabe − *Research Center for Functional Materials, National Institute for Materials Science, Tsukuba 305-0044, Japan;* orcid.org/0000-0003-3701-8119

Takashi Taniguchi − *International Center for Materials Nanoarchitectonics, National Institute for Materials Science, Tsukuba 305-0044, Japan;* orcid.org/0000-0002-1467-3105

Matthew Cothrine − *Material Science & Technology Division, Oak Ridge National Laboratory, Oak Ridge, Tennessee 37831, United States*

David G. Mandrus − *Material Science & Technology Division, Oak Ridge National Laboratory, Oak Ridge, Tennessee 37831, United States;* orcid.org/0000-0003-3616-7104

Chris Jozwiak − *Advanced Light Source, Lawrence Berkeley National Laboratory, Berkeley, California 94720, United States;* orcid.org/0000-0002-0980-3753

Aaron Bostwick − *Advanced Light Source, Lawrence Berkeley National Laboratory, Berkeley, California 94720, United States*

Alexander Weber-Bargioni − *The Molecular Foundry, Lawrence Berkeley National Laboratory, Berkeley, California 94720, United States*

Eli Rotenberg − *Advanced Light Source, Lawrence Berkeley National Laboratory, Berkeley, California 94720, United States;* orcid.org/0000-0002-3979-8844

Complete contact information is available at: https://pubs.acs.org/10.1021/acs.nanolett.3c01974

Author Contributions

The manuscript was written through contributions of all authors. All authors have given approval to the final version of the manuscript.

Notes

The authors declare no competing financial interest.

ACKNOWLEDGMENTS

This work was supported as part of the Center for Novel Pathways to Quantum Coherence in Materials, an Energy Frontier Research Center funded by the U.S. Department of Energy, Office of Science, Basic Energy Sciences. Work was performed at the Molecular Foundry and at the Advanced Light Source, which was supported by the Office of Science, Office of Basic Energy Sciences, of the U.S. Department of Energy under contract no. DE-AC02-05CH11231. A.W.-B. and J.C.T. acknowledge support from the U.S. Department of Energy, Office of Science, National Quantum Information Science Research Center, Quantum Systems Accelerator. A.R. received funding from the European Union's Horizon 2020 research and innovation programme under grant agreement 881603. R.D. performed this work under the auspices of the U.S. Department of Energy by Lawrence Livermore National Laboratory under Contract DE-AC52-07NA27344. E.A.H. acknowledges support by the Office of the Under Secretary of Defense for Research and Engineering under award number FA9550-22-1-0340 and the Moore Foundation Experimental Physics Investigators Initiative award no. 11560. We acknowledge support for device fabrication by the Institute of Materials Science and Engineering at Washington University in St. Louis. The authors thank Dr. Luca Moreschini from University of California, Berkeley and Dr. Stiven Forti from Istituto Italiano di Tecnologia, Pisa for the fruitful discussion.

REFERENCES

(1) Novoselov, K. S.; Mishchenko, A.; Carvalho, A.; Castro Neto, A. H. 2D Materials and van Der Waals Heterostructures. *Science* **2016**, *353* (6298), aac9439.

(2) Liu, Y.; Weiss, N. O.; Duan, X.; Cheng, H.-C.; Huang, Y.; Duan, X. Van Der Waals Heterostructures and Devices. *Nat. Rev. Mater.* **2016**, *1* (9), 1−17.

(3) Pham, P. V.; Bodepudi, S. C.; Shehzad, K.; Liu, Y.; Xu, Y.; Yu, B.; Duan, X. 2D Heterostructures for Ubiquitous Electronics and Optoelectronics: Principles, Opportunities, and Challenges. *Chem. Rev.* **2022**, *122* (6), 6514−6613.

(4) Mak, K. F.; Shan, J. Photonics and Optoelectronics of 2D Semiconductor Transition Metal Dichalcogenides. *Nature Photon* **2016**, *10* (4), 216−226.

(5) Sierra, J. F.; Fabian, J.; Kawakami, R. K.; Roche, S.; Valenzuela, S. O. Van Der Waals Heterostructures for Spintronics and Opto-Spintronics. *Nat. Nanotechnol.* **2021**, *16* (8), 856−868.

(6) Keimer, B.; Moore, J. E. The Physics of Quantum Materials. *Nature Phys.* **2017**, *13* (11), 1045−1055.

(7) Lemme, M. C.; Akinwande, D.; Huyghebaert, C.; Stampfer, C. 2D Materials for Future Heterogeneous Electronics. *Nat. Commun.* **2022**, *13* (1), 1392.

(8) Zhou, B.; Balgley, J.; Lampen-Kelley, P.; Yan, J.-Q.; Mandrus, D. G.; Henriksen, E. A. Evidence for Charge Transfer and Proximate

Magnetism in Graphene-$RuCl_3$ Heterostructures. *Phys. Rev. B* **2019**, *100* (16), 165426.
(9) Biswas, S.; Li, Y.; Winter, S. M.; Knolle, J.; Valentí, R. Electronic Properties of $RuCl_3$ in Proximity to Graphene. *Phys. Rev. Lett.* **2019**, *123* (23), 237201.
(10) Mashhadi, S.; Kim, Y.; Kim, J.; Weber, D.; Taniguchi, T.; Watanabe, K.; Park, N.; Lotsch, B.; Smet, J. H.; Burghard, M.; Kern, K. Spin-Split Band Hybridization in Graphene Proximitized with α-RuCl3 Nanosheets. *Nano Lett.* **2019**, *19* (7), 4659−4665.
(11) Wang, Y.; Balgley, J.; Gerber, E.; Gray, M.; Kumar, N.; Lu, X.; Yan, J.-Q.; Fereidouni, A.; Basnet, R.; Yun, S. J.; Suri, D.; Kitadai, H.; Taniguchi, T.; Watanabe, K.; Ling, X.; Moodera, J.; Lee, Y. H.; Churchill, H. O. H.; Hu, J.; Yang, L.; Kim, E.-A.; Mandrus, D. G.; Henriksen, E. A.; Burch, K. S. Modulation Doping via a Two-Dimensional Atomic Crystalline Acceptor. *Nano Lett.* **2020**, *20* (12), 8446−8452.
(12) Balgley, J.; Butler, J.; Biswas, S.; Ge, Z.; Lagasse, S.; Taniguchi, T.; Watanabe, K.; Cothrine, M.; Mandrus, D. G.; Velasco, J.; Valentí, R.; Henriksen, E. A. Ultrasharp Lateral p-n Junctions in Modulation-Doped Graphene. *Nano Lett.* **2022**, *22* (10), 4124−4130.
(13) Plumb, K. W.; Clancy, J. P.; Sandilands, L. J.; Shankar, V. V.; Hu, Y. F.; Burch, K. S.; Kee, H.-Y.; Kim, Y.-J. α-$RuCl_3$: A Spin-Orbit Assisted Mott Insulator on a Honeycomb Lattice. *Phys. Rev. B* **2014**, *90* (4), 041112.
(14) Sears, J. A.; Songvilay, M.; Plumb, K. W.; Clancy, J. P.; Qiu, Y.; Zhao, Y.; Parshall, D.; Kim, Y.-J. Magnetic Order in α-$RuCl_3$: A Honeycomb-Lattice Quantum Magnet with Strong Spin-Orbit Coupling. *Phys. Rev. B* **2015**, *91* (14), 144420.
(15) Tian, Y.; Gao, W.; Henriksen, E. A.; Chelikowsky, J. R.; Yang, L. Optically Driven Magnetic Phase Transition of Monolayer RuCl3. *Nano Lett.* **2019**, *19* (11), 7673−7680.
(16) Sandilands, L. J.; Tian, Y.; Plumb, K. W.; Kim, Y.-J.; Burch, K. S. Scattering Continuum and Possible Fractionalized Excitations in α-$RuCl_3$. *Phys. Rev. Lett.* **2015**, *114* (14), 147201.
(17) Banerjee, A.; Bridges, C. A.; Yan, J.-Q.; Aczel, A. A.; Li, L.; Stone, M. B.; Granroth, G. E.; Lumsden, M. D.; Yiu, Y.; Knolle, J.; Bhattacharjee, S.; Kovrizhin, D. L.; Moessner, R.; Tennant, D. A.; Mandrus, D. G.; Nagler, S. E. Proximate Kitaev Quantum Spin Liquid Behaviour in a Honeycomb Magnet. *Nat. Mater.* **2016**, *15* (7), 733−740.
(18) Do, S.-H.; Park, S.-Y.; Yoshitake, J.; Nasu, J.; Motome, Y.; Kwon, Y. S.; Adroja, D. T.; Voneshen, D. J.; Kim, K.; Jang, T.-H.; Park, J.-H.; Choi, K.-Y.; Ji, S. Majorana Fermions in the Kitaev Quantum Spin System α-RuCl3. *Nature Phys.* **2017**, *13* (11), 1079−1084.
(19) Kasahara, Y.; Ohnishi, T.; Mizukami, Y.; Tanaka, O.; Ma, S.; Sugii, K.; Kurita, N.; Tanaka, H.; Nasu, J.; Motome, Y.; Shibauchi, T.; Matsuda, Y. Majorana Quantization and Half-Integer Thermal Quantum Hall Effect in a Kitaev Spin Liquid. *Nature* **2018**, *559* (7713), 227−231.
(20) Bruin, J. a. N.; Claus, R. R.; Matsumoto, Y.; Kurita, N.; Tanaka, H.; Takagi, H. Robustness of the Thermal Hall Effect Close to Half-Quantization in α-RuCl3. *Nat. Phys.* **2022**, *18* (4), 401−405.
(21) Kitaev, A. Anyons in an Exactly Solved Model and Beyond. *Annals of Physics* **2006**, *321* (1), 2−111.
(22) Kim, S.; Yuan, B.; Kim, Y.-J. α-RuCl3 and Other Kitaev Materials. *APL Materials* **2022**, *10* (8), 080903.
(23) Kasahara, Y.; Suetsugu, S.; Asaba, T.; Kasahara, S.; Shibauchi, T.; Kurita, N.; Tanaka, H.; Matsuda, Y. Quantized and Unquantized Thermal Hall Conductance of the Kitaev Spin Liquid Candidate α-$RuCl_3$. *Phys. Rev. B* **2022**, *106* (6), L060410.
(24) Gerber, E.; Yao, Y.; Arias, T. A.; Kim, E.-A. Ab Initio Mismatched Interface Theory of Graphene on α-$RuCl_3$: Doping and Magnetism. *Phys. Rev. Lett.* **2020**, *124* (10), 106804.
(25) Choi, W.; Klein, P. W.; Rosch, A.; Kim, Y. B. Topological Superconductivity in the Kondo-Kitaev Model. *Phys. Rev. B* **2018**, *98* (15), 155123.
(26) Seifert, U. F. P.; Meng, T.; Vojta, M. Fractionalized Fermi Liquids and Exotic Superconductivity in the Kitaev-Kondo Lattice. *Phys. Rev. B* **2018**, *97* (8), 085118.
(27) Leeb, V.; Polyudov, K.; Mashhadi, S.; Biswas, S.; Valentí, R.; Burghard, M.; Knolle, J. Anomalous Quantum Oscillations in a Heterostructure of Graphene on a Proximate Quantum Spin Liquid. *Phys. Rev. Lett.* **2021**, *126* (9), 097201.
(28) Rizzo, D. J.; Shabani, S.; Jessen, B. S.; Zhang, J.; McLeod, A. S.; Rubio-Verdú, C.; Ruta, F. L.; Cothrine, M.; Yan, J.; Mandrus, D. G.; Nagler, S. E.; Rubio, A.; Hone, J. C.; Dean, C. R.; Pasupathy, A. N.; Basov, D. N. Nanometer-Scale Lateral p-n Junctions in Graphene/α-RuCl3 Heterostructures. *Nano Lett.* **2022**, *22* (5), 1946−1953.
(29) Rizzo, D. J.; Jessen, B. S.; Sun, Z.; Ruta, F. L.; Zhang, J.; Yan, J.-Q.; Xian, L.; McLeod, A. S.; Berkowitz, M. E.; Watanabe, K.; Taniguchi, T.; Nagler, S. E.; Mandrus, D. G.; Rubio, A.; Fogler, M. M.; Millis, A. J.; Hone, J. C.; Dean, C. R.; Basov, D. N. Charge-Transfer Plasmon Polaritons at Graphene/α-RuCl3 Interfaces. *Nano Lett.* **2020**, *20* (12), 8438−8445.
(30) Romagnoli, M.; Sorianello, V.; Midrio, M.; Koppens, F. H. L.; Huyghebaert, C.; Neumaier, D.; Galli, P.; Templ, W.; D'Errico, A.; Ferrari, A. C. Graphene-Based Integrated Photonics for next-Generation Datacom and Telecom. *Nat. Rev. Mater.* **2018**, *3* (10), 392−414.
(31) Rotenberg, E.; Bostwick, A. MicroARPES and NanoARPES at Diffraction-Limited Light Sources: Opportunities and Performance Gains. *J. Synchrotron Rad* **2014**, *21* (5), 1048−1056.
(32) Yu, Y.-J.; Zhao, Y.; Ryu, S.; Brus, L. E.; Kim, K. S.; Kim, P. Tuning the Graphene Work Function by Electric Field Effect. *Nano Lett.* **2009**, *9* (10), 3430−3434.
(33) Zhou, X.; Li, H.; Waugh, J. A.; Parham, S.; Kim, H.-S.; Sears, J. A.; Gomes, A.; Kee, H.-Y.; Kim, Y.-J.; Dessau, D. S. Angle-Resolved Photoemission Study of the Kitaev Candidate α-$RuCl_3$. *Phys. Rev. B* **2016**, *94* (16), 161106.
(34) Doniach, S.; Sunjic, M. Many-Electron Singularity in X-Ray Photoemission and X-Ray Line Spectra from Metals. *J. Phys. C: Solid State Phys.* **1970**, *3* (2), 285.
(35) Joucken, F.; Avila, J.; Ge, Z.; Quezada-Lopez, E. A.; Yi, H.; Le Goff, R.; Baudin, E.; Davenport, J. L.; Watanabe, K.; Taniguchi, T.; Asensio, M. C.; Velasco, J., Jr Visualizing the Effect of an Electrostatic Gate with Angle-Resolved Photoemission Spectroscopy. *Nano Lett.* **2019**, *19* (4), 2682−2687.
(36) Sinn, S.; Kim, C. H.; Kim, B. H.; Lee, K. D.; Won, C. J.; Oh, J. S.; Han, M.; Chang, Y. J.; Hur, N.; Sato, H.; Park, B.-G.; Kim, C.; Kim, H.-D.; Noh, T. W. Electronic Structure of the Kitaev Material α-RuCl3 Probed by Photoemission and Inverse Photoemission Spectroscopies. *Sci. Rep* **2016**, *6* (1), 39544.
(37) Shirley, E. L.; Terminello, L. J.; Santoni, A.; Himpsel, F. J. Brillouin-zone-selection effects in graphite photoelectron angular distributions. *Phys. Rev. B* **1995**, *51* (19), 13614.
(38) Luttinger, J. M. Fermi Surface and Some Simple Equilibrium Properties of a System of Interacting Fermions. *Phys. Rev.* **1960**, *119* (4), 1153−1163.
(39) Bostwick, A.; Ohta, T.; Seyller, T.; Horn, K.; Rotenberg, E. Quasiparticle Dynamics in Graphene. *Nature Phys.* **2007**, *3* (1), 36−40.
(40) Rosenzweig, P.; Karakachian, H.; Marchenko, D.; Küster, K.; Starke, U. Overdoping Graphene beyond the van Hove Singularity. *Phys. Rev. Lett.* **2020**, *125* (17), 176403.

https://doi.org/10.1021/acs.nanolett.3c01974
Nano Lett. 2023, 23, 8000−8005